SnO_2 coated Ni particles prepared by fluidized bed chemical vapor deposition

N. Bertrand [a,*], F. Maury [b], P. Duverneuil [a]

[a] *Laboratoire de Génie Chimique (LGC), CNRS/INPT/UPS, BP 1301, 5 rue Paulin Talabot, 31106 Toulouse cedex 1, France*
[b] *Centre Interuniversitaire de Recherche et d'Ingénierie des Matériaux (CIRIMAT), CNRS/INPT, ENSIACET, 118 route de Narbonne, 31077 Toulouse cedex 4, France*

Abstract

A Fluidized Bed Metal–Organic Chemical Vapor Deposition (FB-MOCVD) process was developed for the growth of tin oxide thin films on large hollow Ni particles. Tetraethyl tin was used as tin source and dry air both as fluidization gas and oxidant reagent. The SnO_2 films were grown in a FBCVD reactor under reduced pressure (13.3 kPa) in the temperature range of 633–663 K. A series of specific experiments was carried out to optimize the design of the reactor and to determine the range of experimental parameters (flow rate, pressure, temperature) leading to good fluidization of the large hollow Ni particles used as base material. The SnO_2 films deposited on particles exhibited a dense nodular surface morphology similar to that previously observed on flat substrates. The relative thickness of the films was determined by EDS analyses and the real values were measured by SEM on cross-sections of particles. The SnO_2 films exhibit satisfactory thickness uniformity from one particle to another in the same batch and from run to run. XRD studies revealed that the films exhibited good crystallinity with the cassiterite structure. Traces of NiO were found at the SnO_2/Ni interface. Finally, the SnO_2 CVD coated-Ni particles were used as anodes in an electrochemical cell. The potential limit of oxygen evolution measured was that of the SnO_2 layer despite the initial porosity of the hollow Ni particles inherent to their preparation. This work is the first step towards the preparation of high specific surface area electrodes.

Keywords: Organometallic CVD; Fluidized bed CVD; Tin oxide; Anode material

1. Introduction

Tin oxide thin films have important applications due to their semi-conductive properties and to their optical transmission. The main application concerns gas sensors, owing to the strong dependence of the conductivity of the films on the ambient atmosphere and on the temperature [1,2]. Recent works deal with the development of SnO_2 films as electrochemical materials. SnO_2 thin films have been successfully used as anode material in an electrochemical process for the depollution of organic compounds in wastewater. Conventional anodes, such as Pt, Ti/IrO_x, Ti/RuO_2 and Ti/PbO_2, give relatively low current efficiencies in contrast to the SnO_2 anode, which not only gives high current efficiency, but also allows quasi complete total organic carbon (TOC) elimination [3,4]. Furthermore, the electrochemical method for wastewater treatment is easy to control and its efficiency could be significantly increased by the use of electrodes with a higher specific surface area.

Thin films of SnO_2 have been deposited by a variety of techniques including reactive sputtering [5], spray pyrolysis [6], evaporation [7], sol–gel [8], pulsed Laser deposition [9], plasma-assisted chemical vapor deposition [10] and thermal chemical vapor deposition (CVD). Among these techniques, CVD has meaningful advantages such as its capacity for large area growth, precise control of thickness and superior conformal coverage. The use of labile organometallic molecules allows deposition of thin films at low temperatures that most inorganic substrates can tolerate.

The aim of this work was to prepare specific electrodes by metal–organic chemical vapor deposition of SnO_2 on Ni particles in a fluidized bed reactor (FB-MOCVD). In previous

* Corresponding author. Present address: Laboratoire des Composites Thermostructuraux (LCTS), UMR 5801 CNRS/SNECMA/CEA/UB1, 3 allée de la Boétie, 33600 Pessac, France. Tel.: +33 556 844 735; fax: +33 556 841 225.
E-mail address: bertrand@lcts.u-bordeaux1.fr (N. Bertrand).

doi:10.1016/j.surfcoat.2005.10.009

works we have reported optimal CVD conditions for the growth of SnO_2 on flat substrates [11–13]. SnO_2 thin films were grown by MOCVD at 653 K and 13.3 kPa using tetraethyl tin ($SnEt_4$) as molecular precursor with a mole fraction of 10^{-3} and oxygen as oxidant reagent [13]. In the present work, the deposition of SnO_2 was done on hollow Ni particles in a fluidized bed reactor. The use of a fluidized bed reactor has great advantages for the CVD technique [14]. One of the most important features is the relatively large heat and mass transfer rates. Consequently, the temperature and the gas composition in the bed are more homogeneous than in a conventional CVD reactor. By setting the global parameters of the process (*T*, *P*, flow rates and mole fraction of the reactants), the local growth conditions are well controlled and the fluidization phenomena lead to a good thickness uniformity of the coatings.

2. Experimental

Calculations and several series of specific experiments were performed to design and to build the fluidized bed CVD reactor used for SnO_2 deposition. The process is related to the MOCVD process previously developed for coating flat substrates [11–13]. Basically, $SnEt_4$ was used as tin source and dry air both as fluidization gas and oxidant.

2.1. Selection and preparation of the substrate

The substrate was chosen (i) to provide a high electrocatalytic efficiency and (ii) to be easily fluidized in the CVD reactor. The first requirement results from the application for these coated particles: the substrate coated by SnO_2 will be immersed in an electrochemical reactor as anode material for the depollution of wastewater [15]. Consequently, its density must be higher than that of water. Furthermore, the diameter of the particles used as substrates must be large enough to offer both the high surface area required for an efficient organic degradation and sufficient electrical conductivity to use the material as an anode. Titanium is frequently used as base material for electrode fabrication and CVD of SnO_2 films on Ti plates have already been reported [16]. However, Ti particles are quite expensive and preliminary fluidization attempts were not satisfactory. Taking into account economical factors in addition to the above requirements, Ni appeared to be a good candidate. Indeed, it has been used as an electrode material in various electrochemical processes [17].

Regarding the second item, the particles to be coated must be fluidized homogeneously to carry out a reliable CVD process. However, fluidization of large particles under reduced pressure is difficult and generally tends to operate in the slugging regime [18]. As a result, a good compromise was the use of hollow Ni particles as substrates, 2.17 mm in mean diameter and 2160 kg m^{-3} in density. These particles belong to the D group according to the Geldart classification [19]. The typical behavior ascribed to the D group is a rapid increase of the bubble size with the bed height, which causes strong interactions between the bubbles themselves and the reactor walls. Such flow conditions promote the formation of slugs, which are usually described as square-nosed slugs or solids slugs [20].

The hollow Ni particles underwent various treatments before their use as substrates in the FBCVD process. They were degreased with trichloroethylene and acetone and dried at 353 K for 10 min. Part of the particles were separated and precoated with a thin layer of IrO_x deposited by dip-coating [21]. The process involved the following steps: the Ni particles were dipped in an isopropanol solution of $IrCl_4$ (15 wt.%), the solvent was evaporated at 353 K for 10 min and the samples were heated in air at 773 K for 5 min. The above operations were repeated three times to improve the uniformity and the thickness of the IrO_x coating. Finally, the particles were annealed in air at 773 K for 1 h.

2.2. Design of the fluidized bed CVD reactor

The reactor was designed to avoid or to limit slugging behavior. It is known that increasing the reactor diameter changes the total slugging regime towards wall slugs then axisymmetric slugs, as frequently observed in systems with small particle sizes [22]. However, an increase in the reactor diameter requires a higher tetraethyl tin flow rate and, consequently, higher consumption of the metal–organic precursor. A reactor diameter of 5 cm was found to be a good compromise because of the relatively high cost of the molecular precursor.

The distributor at the bottom of the reactor was a porous or perforated plate serving both as support for the bed of granular material and as a uniform diffuser of the gas stream through the bed. A high porosity plate generally reduces the slugging behavior [23]. In this work, the gas distributor was a perforated stainless steel plate with a porosity of 30%. For some experiments, a half cone-shaped stainless steel piece (5 cm diameter) was placed on a part of the gas distributor to produce a spouted bed regime.

The MOCVD set-up is depicted in Fig. 1. The decomposition and oxidation reactions of $SnEt_4$ took place in a fluidized

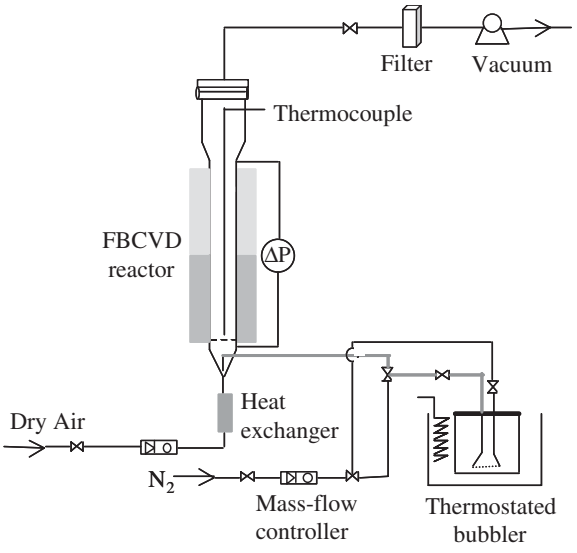

Fig. 1. Schematic representation of the FBCVD reactor.

bed reactor entirely constructed from a 304-L stainless steel; its dimensions were 1 m height and 0.05 m internal diameter and it was closed at the bottom by the perforated plate. Heating was provided by an electrical resistance furnace. Typically, the temperature profile revealed a difference from the bottom to the top of the particle bed of 30° for a furnace temperature of 653 K. This temperature gradient is due to the relatively high total flow rate required to fluidize the large Ni particles.

Tetraethyl tin is a liquid compound in the operating conditions. It was transported as vapor from a thermostated bubbler to the reactor using an inert carrier gas (N_2). The gas streams (N_2 and dry air) were monitored using mass flow meters. The total pressure in the reactor was controlled automatically using an absolute pressure gauge coupled to a throttle valve control system.

The mole fraction of $SnEt_4$ (10^{-3}) and the total pressure (13.3 kPa) in the reactor were fixed at the values determined in a previous kinetic study carried out on flat substrates [11,12]. The total gas flow rate (2.16×10^{-4} Nm^3/s) was deduced from preliminary fluidization experiments (Section 3.1). The mole fraction of $SnEt_4$ was adjusted from the N_2 and air flow rates and from the dependence of $SnEt_4$ vapor pressure on the temperature according to the Clausius–Clapeyron equation [24]:

$$\log P_{\mathrm{sat}}\ (\mathrm{kPa}) = 7.369 - \frac{2448}{T\ (\mathrm{K})}.$$

In FBCVD a more uniform film thickness is expected when the process is kinetically controlled by mass transfer rather than by chemical reactions [14]. Previous kinetic studies performed using this reactive gas mixture indicated that a large excess of oxygen was necessary for kinetic control of the process by mass transfer. This was achieved typically for a mole ratio $O_2/SnEt_4 \geq 200$ [11,12]. In the present work, the $O_2/SnEt_4$ ratio was fixed at 197 by combining proper flow rates and bubbler temperatures. The optimal SnO_2 growth conditions are reported in Table 1.

2.3. General instrumentation

The surface morphology and microstructure of SnO_2 films and IrO_x underlayers were investigated by scanning electron microscopy (SEM) and XRD (Cu Kα). The samples were analyzed by means of energy dispersion spectrometry (EDS). The thickness uniformity of the SnO_2 films was checked from the relative thicknesses determined by EDS from the Sn/Ni intensity ratios. The thickness of the SnO_2 films was measured on particle cross-sections by SEM.

Table 1
Typical operating conditions for the FBCVD growth of SnO_2 thin films on hollow Ni particles

Deposition temperature (K)	633–663
Total pressure (kPa)	13.3
$SnEt_4$ mole fraction	10^{-3}
Initial bed height (m)	0.20
Bubbler temperature (K)	333
N_2 flow rate (Nm^3/s)	2.77×10^{-6}
Air flow rate (Nm^3/s)	2.13×10^{-4}
$O_2/SnEt_4$ mole ratio	197

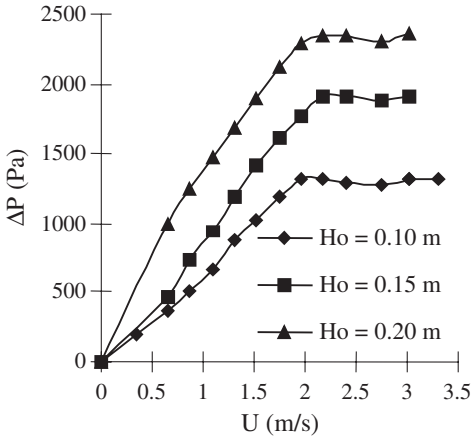

Fig. 2. Pressure drop versus total gas velocity in a spouted-bed CVD reactor measured for different initial bed heights (H_0) of Ni particles.

Electrochemical characterizations were performed by voltamperometry in a three-electrode cell with a working electrode, an ECS reference electrode (saturated Hg/Hg_2Cl_2, saturated KCl) and a platinum auxiliary electrode. The electrolyte solution (0.14 M Na_2SO_4) was maintained at room temperature and mechanically stirred during the voltamperometry test.

3. Results and discussion

3.1. Fluidization conditions without CVD reaction

A series of experiments was performed under reduced pressure in a Pyrex column 5 cm in diameter in order to determine optimal fluidization conditions. The pressure drop versus total gas velocity was measured to evaluate the minimum fluidization velocity of Ni particles. These measurements coupled to observations of the behavior of the fluidized bed as a function of the total gas velocity enabled the existence of the various fluidization regimes to be confirmed.

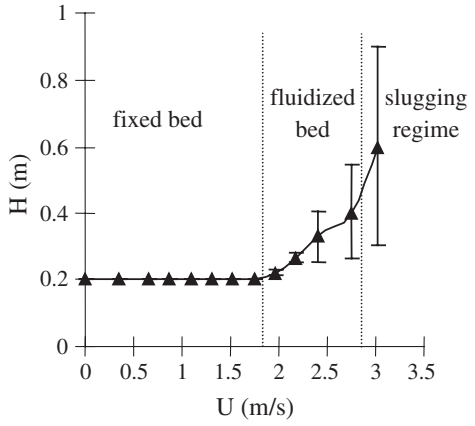

Fig. 3. Bed expansion (H) versus total gas velocity for initial bed height H_0=0.20 m showing the different regimes of the CVD reactor.

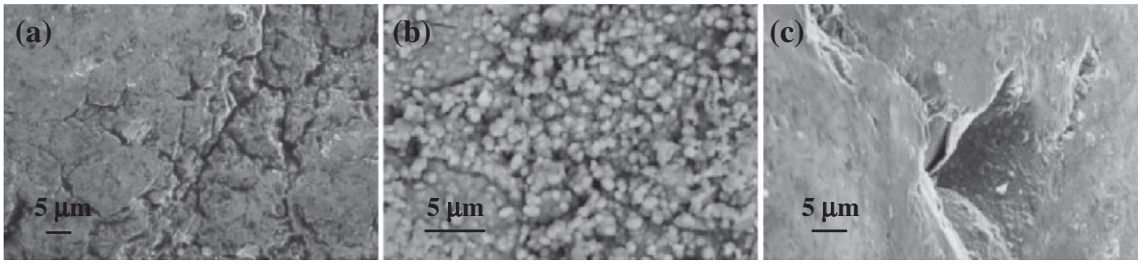

Fig. 4. Typical SEM micrographs of the surface of (a) as-received Ni particle, (b) SnO_2 layer deposited under optimal growth conditions (thickness = 2.2 µm) and (c) SnO_2 layer showing a good conformal coverage of the edges of open pores of the hollow Ni particles but also sometimes a detachment from the substrate in these defects.

The first experiments concerned the fluidization of Ni particles under reduced pressure with the 30% porosity perforated plate. The influence of initial bed height (H_0) on the existence of slugging regime was investigated. Three initial bed heights were tested (0.10 m, 0.15 m and 0.20 m). The occurrence of wall slugs was observed for low values of H_0 (0.10 m), which is generally characteristic of small particles. For higher values of H_0, the bed tended to operate in a slugging regime of large particles with solids slugs. This means the bubbles coalesced to form a single bubble whose diameter was as large as the reactor diameter. Consequently, the measurements of pressure drop versus total gas velocity were no longer linear but exhibited an irregular oscillatory behavior. The occurrence of solid slugs must be avoided because it greatly lowers the homogeneity of the mixing and the quality of gas–particle contact. Moreover, a fluidized bed in the slugging regime generates intense attrition between the fluidized particles and the reactor walls. All these disadvantages must be avoided during the growth process.

In a second series of experiments, a spouted-bed reactor was tested. In this configuration, whatever the initial bed height, the slugging phenomena were significantly reduced. The solids slugs previously observed became wall slugs. Pressure drops versus superficial gas velocity were measured for different initial bed heights (0.10 m, 0.15 m and 0.20 m) and the results are reported in Fig. 2. Bed expansion was also evaluated versus superficial gas velocity for the highest H_0 tested (Fig. 3).

The experimental value of the minimum fluidization velocity of large Ni particles was determined under low pressure from the experimental data reported in Fig. 2. A value of 2 m/s was found. The maximum volume of particles that can be treated corresponded to approximately $H_0 = 0.20$ m. This volume was limited by the total height of the reactor and by the existence of slugging regime at higher bed height. For a gas velocity of 3 m/s, bed expansion reached the top of the reactor (Fig. 3).

3.2. FBCVD of SnO_2

Once the fluidization conditions had been determined, preliminary CVD runs were performed to check the set-up and optimize the growth parameters. Therefore, the heat exchanger for air was slightly modified to provide a more isothermal profile. The minimum fluidization velocity increased slightly with the temperature as mentioned in [25]. As a consequence, the flow rates had to be changed. Thereafter the CVD runs were carried out under the optimal operating conditions reported in Table 1.

The surface morphology of as-received Ni particles exhibited relatively high roughness and defects such as cracks and pores (Fig. 4a). The SnO_2 layers deposited under optimal FBCVD conditions were dense and made up of nodular grains with a mean grain size of approximately 500 nm (Fig. 4b). This microstructure is in good agreement with previous results

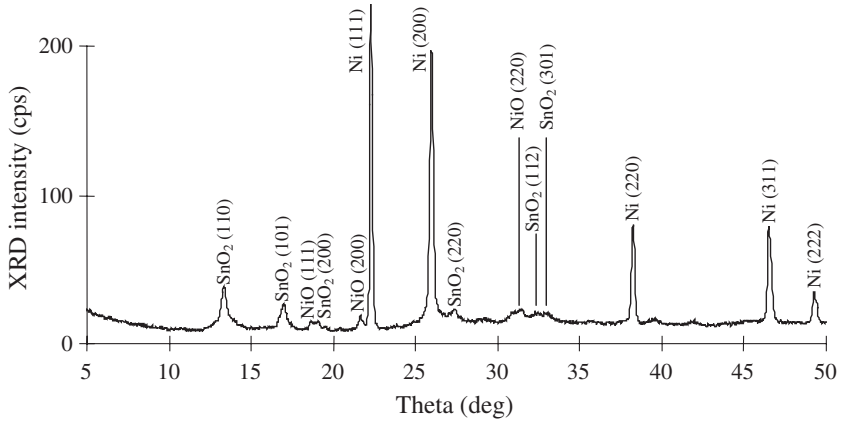

Fig. 5. X-ray diffraction pattern of the SnO_2 layer deposited under optimal growth conditions showing the presence of NiO at the SnO_2/Ni interface (SnO_2 thickness = 2.2 µm).

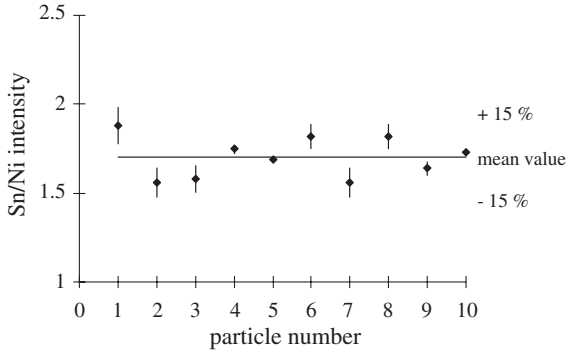

Fig. 6. Typical EDS analysis of 10 SnO_2-coated Ni particles taken at random from the bed of the same CVD run. The Sn/Ti intensity ratio reveals a relatively good thickness uniformity.

obtained for SnO_2 films grown by LPCVD on flat substrates [13]. The SnO_2 layers exhibit a good conformal coverage of the edges of the pores but SnO_2 was probably not deposited on the inner wall of the hollow Ni particles. For some particles the SnO_2 layer was seen to become detached around such defects (Fig. 4c).

A typical X-ray diffraction pattern of SnO_2-coated Ni particles is reported in Fig. 5. All the diffraction peaks of SnO_2 were identified in addition to those of Ni and traces of NiO. The formation of NiO probably occurs in the first steps of the CVD process. Indeed, before the growth of SnO_2, the Ni particles are fluidized using an air stream and are heated in this oxidizing atmosphere until the temperature profile is established. In addition, the Ni particles can also be oxidized during the first stages of SnO_2 growth before tin oxide completely covers the Ni particles. The formation of nickel oxide on the Ni particles does not prevent the use of these treated particles as anode materials because NiO exhibits a sufficiently high conductivity and its formation in this CVD process is quite limited. It is a p-type semi-conductor that has been used previously as electrode material for various electrochemical processes [17].

The SnO_2 films had a microcrystalline structure with a mean grain size of approximately 500 nm. They exhibited the cassiterite structure and no other tin oxide phase was found. The relative intensity of XRD peaks gave no evidence for a preferential orientation of the SnO_2 crystallites, but this was difficult to observe on these non-flat substrates. The crystallite size estimated from the FWHM of the (110) SnO_2 reflection was about 60 nm. This value is in good agreement with a previous study on flat substrates [13]. The mean size of the nodular grains estimated by SEM was significantly higher (500 nm) indicating that the nodules are constituted of agglomerated nanocrystallites.

The EDS spectra revealed only the expected elements Sn, O, Ni and Ir (when IrO_x was deposited prior to SnO_2 deposition). Keeping the EDS conditions constant, the intensity ratio Sn/Ni is related to the thickness of SnO_2. As a result, EDS was used as non-destructive diagnostic technique to determine the thickness uniformity from one particle to another in the same batch and from run to run. Typically, Fig. 6 shows the relatively good uniformity of SnO_2 thickness for 10 coated particles taken at random in the bed from the same CVD run. The Sn/Ni intensity ratio did not exceed ±15%. Similarly, satisfactory reproducibility was found from run to run.

The IrO_x underlayer deposited by dip-coating prior to SnO_2 CVD was found amorphous by X-ray diffraction. Furthermore, SEM observations revealed a dry-mud like morphology with irregular blocks separated by a network of large cracks. These observations are in agreement with the results reported on flat substrates [16]. EDS analyses coupled with SEM were performed on IrO_x-coated Ni particles before fluidization and on $Ni/IrO_x/SnO_2$ particles prepared by a process combining dip coating IrO_x and FBCVD of SnO_2. This study clearly

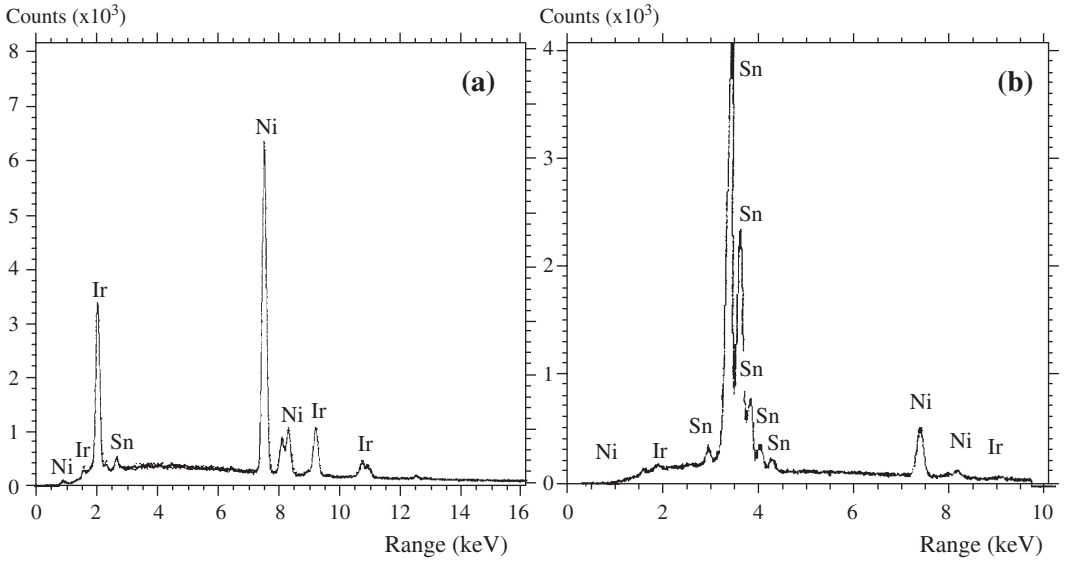

Fig. 7. Typical EDS spectra of (a) IrO_x-coated Ni particles before fluidization and (b) of $Ni/IrO_x/SnO_2$ particles prepared by FBCVD showing that most of the IrO_x underlayer was lost during the fluidized process.

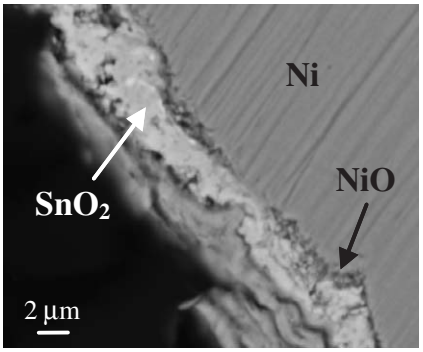

Fig. 8. SEM image of the cross-section of a Ni/IrO_x/SnO_2 particle.

revealed that the relative intensity of Ir was strongly reduced after deposition of SnO_2 by FBCVD (Fig. 7). This was certainly due to loss of IrO_x in the fluidized bed as a result of a poor adhesion of IrO_x to the Ni particles. Indeed, decohesive failure of IrO_x occurs during the fluidization of the Ni particles due to friction between the particles themselves and with the reactor wall. As a result, a large part of the IrO_x layer was lost in the early stages of the FBCVD process and most of the SnO_2 coating grew directly on the Ni surface. Obviously, as for the untreated Ni particles, the oxidizing atmosphere prior to the deposition of SnO_2 led to the formation of NiO on their surface.

Fig. 8 shows a SEM micrograph of a typical cross-section of a Ni/IrO_x/SnO_2 particle. The presence of IrO_x at the interface between Ni and SnO_2 was difficult to observe in some areas. Only the presence of fragments containing Ir was found, which confirms that only traces of the IrO_x layer remained. Different contrast at the Ni/SnO_2 interface revealed the presence of NiO. The SnO_2 coating was dense and exhibited a good conformal coverage of the relief as found for SnO_2 growth on flat Ti substrates [16]. From the mean thickness of SnO_2 a typical growth rate of 6 nm/min was determined in good agreement with previous work [13]. The comparable growth rates on flat substrates in an MOCVD process and on particles in an FBCVD reactor indicates that the process is kinetically controlled by mass transfer rather than by chemical reactions. Actually, the mole ratio $O_2/SnEt_4$ of 197 provided a sufficient excess of oxygen in the gas stream for the process to operate in this kinetic regime.

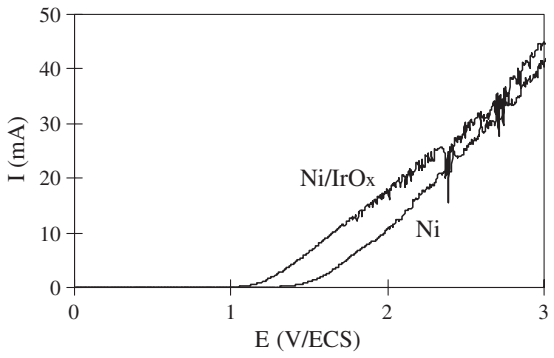

Fig. 9. Characteristic voltamperograms of Ni and IrO_x-coated Ni anodes.

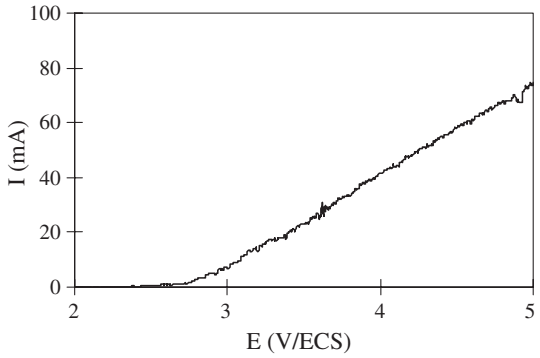

Fig. 10. Characteristic voltamperogram of a Ni/SnO_2 particle used as anode. The particle was treated with IrO_x prior to FBCVD but only traces of this oxide were present on the final anode.

3.3. Electrochemical properties

The electrochemical characterizations were performed by linear voltamperometry. This consisted in measuring anodic potential versus current intensity. The potential limit of oxygen evolution depends on the anodic material [26]. This electrochemical technique permits the identification of the electrochemically active layer. SnO_2 has to be electrochemically active in order to efficiently destroy organic pollutants by electrochemical oxidation. The electrochemical cell used for these characterizations contained a Ni particle coated by IrO_x and SnO_2 as anode, a platinum grid as cathode and an ECS as reference electrode.

The first electrochemical experiments consisted in determining the anodic potential of oxygen evolution for Ni and Ni/IrO_x anodes. The typical voltamperograms, reported in Fig. 9, revealed an anodic potential of oxygen evolution for a Ni anode of 1.5 V/ECS and for an IrO_x-coated Ni anode of 1.2 V/ECS.

After the base materials, several Ni/IrO_x/SnO_2 particles were characterized by linear voltamperometry. The characteristic voltamperogram reported in Fig. 10 indicates an oxidation reaction for a potential value of about 2.7 V/ECS. This is significantly different from the values found for Ni and IrO_x anodes. Previous work reported an anodic potential of oxygen evolution of 2.82 V/ECS for a SnO_2 anode [27]. This demonstrates that tin dioxide is most likely the electrochemically active layer. However, not all the tested particles prepared by FBCVD exhibited this behavior. Some presented the anodic potential of oxygen evolution of either Ni or Ni/IrO_x anodes. This low reproducibility is probably due on one hand to large pores through the shell of the hollow Ni particles that prevent complete coating of the Ni surface and, on the other hand, to the fact that most of the IrO_x is lost after the FBCVD process.

4. Conclusion

An FBCVD process was developed to deposit SnO_2 thin films on Ni particles. The feasibility of this deposition process was evaluated by preliminary fluidization experiments. The slugging behavior, which is predominant for large Ni particles,

was reduced to wall slugs by the use of a high porosity distributor and by fluidization in a spouted-bed reactor. The fluidization conditions of the hollow Ni particles in the spouted-bed were found suitable to carry out SnO_2 CVD runs.

The thickness uniformity of the SnO_2 films on the particles of one batch or from run to run was found satisfactory. The morphology of SnO_2 consisted of nodular grains, with a mean size of about 500 nm. The SnO_2 thin films are microcrystalline, untextured and exhibit the cassiterite structure. The formation of NiO during the first stages of the process was revealed by XRD analyses. Several $Ni/IrO_x/SnO_2$ particles were used as anodes in an electrochemical cell. The anodic potential measured during oxygen evolution was that of the SnO_2 layer except for some particles that inconsistently exhibited the anodic potential of either Ni or Ni/IrO_x particles. This was probably due to either a large number of pores through the shell of the base material, excessively large defects in the shell, or the poor quality of the IrO_x underlayer grown by dip-coating.

These results show that SnO_2 thin film can act as an anodic material for the electro-oxidation of organic pollutants as demonstrated on flat electrodes [16]. We are continuing our effort to improve the reproducibility of the fabrication of these volumetric $Ni/IrO_x/SnO_2$ anodes by FBCVD, especially by improving the base material (porosity) and the quality of the IrO_x underlayer in order to get better protection of the particles against oxidation in the early stages of the FBCVD process.

References

[1] E. Comini, A. Cristalli, G. Faglia, G. Sberveglieri, Sens. Actuators, B, Chem. 65 (2000) 260.
[2] A.K. Mukhopadhyay, P. Mitra, A.P. Chatterjee, H.S. Maiti, Ceram. Int. 26 (2000) 123.
[3] C. Comninellis, C. Pulgarin, J. Appl. Electrochem. 21 (1991) 703.
[4] C. Comninellis, Trans. IChemE 70 (1992) 219.
[5] T. Maruyama, H. Akagi, J. Electrochem. Soc. 143 (1996) 283.
[6] G. Gordillo, L.C. Moreno, W. de la Cruz, P. Teheran, Thin Solid Films 252 (1994) 61.
[7] W. Hellmich, C.B. Braunmuhl, G. Muller, G. Sberveglieri, M. Berti, C. Perego, Thin Solid Films 263 (1995) 231.
[8] J.P. Chatelon, C. Terrier, E. Bernstein, R. Berjoan, J.A. Roger, Thin Solid Films 247 (1994) 162.
[9] V.P. Godbole, R.D. Vispute, S.M. Chaudhari, S.M. Kanetkar, S.B. Ogale, J. Mater. Res. 5 (1990) 372.
[10] Y.P. Chen, Z.Q. Zheng, S.Y. Li, H.L. Ma, J. Phys., Coll. C5 (50) (1989) 605.
[11] M. Amjoud, F. Maury, M. Elaatmani, Ann. Chim. Sci. Matér. 23 (1998) 355.
[12] M'B. Amjoud, F. Maury, S. Soukane, P. Duverneuil, Surf. Coat. Technol. 100–101 (1998) 169.
[13] N. Bertrand, P. Duverneuil, M'B. Amjoud, F. Maury, J. Phys., IV France 9 (1999) Pr8-651.
[14] S. Kinkel, G.N. Angelopoulos, D.C. Papamantellos, W. Dahl, Mater. Technol., Steel Res. 66 (1995) 318.
[15] O. Simond, V. Schaller, C. Comninellis, Electrochim. Acta 42 (1997) 2009.
[16] P. Duverneuil, F. Maury, N. Pebere, F. Senocq, H. Vergnes, Surf. Coat. Technol. 151–152 (2002) 9.
[17] M. Yoshikawa, Y. Mugikura, T. Watanabe, T. Kahara, T. Mizukami, J. Electrochem. Soc. 148 (2001) A1230.
[18] J. Baeyens, D. Geldart, Chem. Eng. Sci. 29 (1974) 255.
[19] D. Geldart, Powder Technol. 7 (1973) 285.
[20] R. Clift, J.R. Grace, J.F. Davidson (Eds.), Fluidization, Academic Press, 1985, p. 73.
[21] G.P. Vercesi, J.Y. Salamin, C. Comninellis, Electrochim. Acta 36 (1991) 991.
[22] W.J. Thiel, O.E. Potter, Ind. Eng. Chem. Fundam. 16 (1977) 242.
[23] R.C. Darton, R.D. Lanauze, J.F. Davidson, D.D. Harrison, Trans. Inst. Chem. Eng. 55 (1977) 274.
[24] J. Buckingham (Ed.), Dictionary of Organic Compounds, 5th ed., Chapman and Hall, New York, 1982.
[25] G. Flamant, N. Fatah, D. Steinmetz, B. Murachman, C. Laguérie, Entropie 146–147 (1989) 93.
[26] S. Trassati, in: J. Lipkowski, P.N. Ross (Eds.), The Electrochemistry of Novel Materials, 1994, p. 207.
[27] B. Correa-Lozano, C. Comninellis, A. De Battisti, J. Electrochem. Soc. 26 (1996) 683.